IEEE Access
Multidisciplinary | Rapid Review | Open Access Journal

Received February 20, 2019, accepted February 27, 2019, date of publication March 4, 2019, date of current version March 20, 2019.

Digital Object Identifier 10.1109/ACCESS.2019.2902570

Tradeoff Between Secrecy Capacity and Harvested Energy for Secure Visible Light Communications With SWIPT

JIN-YUAN WANG[1,2], (Member, IEEE), SHENG-HONG LIN[1,3], YU QIU[4], NUO HUANG[4], (Student Member, IEEE), AND JUN-BO WANG[4], (Member, IEEE)

[1]Key Lab of Broadband Wireless Communication and Sensor Network Technology, Nanjing University of Posts and Telecommunications, Nanjing 210003, China
[2]Key Laboratory (Research Base) of Signal and Information Processing, Xihua University, Chengdu 610039, China
[3]School of Automation Engineering, Nanjing Institute of Mechatronic Technology, Nanjing 211135, China
[4]National Mobile Communications Research Laboratory, Southeast University, Nanjing 210096, China

Corresponding author: Jun-Bo Wang (jbwang@seu.edu.cn)

This work was supported in part by the National Natural Science Foundation of China under Grant 61701254, Grant 6157115, and Grant 61602235, in part by the Natural Science Foundation of Jiangsu Province under Grant BK20170901 and Grant BK20161007, in part by the Key International Cooperation Research Project under Grant 61720106003, in part by the Open Research Fund of Key Lab of Broadband Wireless Communication and Sensor Network Technology, Nanjing University of Posts and Telecommunications, Ministry of Education, under Grant JZNY201706, in part by the NUPTSF under Grant NY216009, in part by the Open Research Fund for Jiangsu Key Laboratory of Traffic and Transportation Security, Huaiyin Institute of Technology, under Grant TTS2017-03, in part by the Open Research Fund of Key Laboratory of Intelligent Computing and Signal Processing, Anhui University, and in part by the Open Research Subject of Key Laboratory (Research Base) of Signal and Information Processing, Xihua University, under Grant szjj2017-047.

ABSTRACT By considering the threefold roles of indoor visible light communications (VLC), i.e., illumination, secure information transmission, and light power transfer, the tradeoff between the secrecy capacity (SC) and the harvested energy (HE) is investigated in this paper. An indoor VLC system consisting of a transmitter, a legitimate receiver, and an eavesdropper is established. The legitimate receiver can perform secure information transmission and light power transfer simultaneously, while the eavesdropper is just an information eavesdropping receiver. Under the non-negativity and the dimmable average optical intensity constraint, a lower bound of the average SC is derived. By employing the dynamic power splitting (DPS) for the legitimate receiver, the closed-form expression of the average HE is obtained. After that, the SC-HE region for the DPS receiver is constructed. As the variants of the DPS receiver, the time switching (TS), static power splitting (SPS) and on–off power splitting (OPS) receivers are provided, and the corresponding SC-HE regions are also obtained. As a benchmark, the performance upper bound of the SC-HE region for any practical receiver is derived. The simulation results show that the performance of the OPS receiver always outperforms that of the other receivers. The DPS and SPS receivers achieve the same performance. The TS receiver is the worst receiver when HE is small, but it is the best receiver when HE is large. Moreover, the impacts of the dimming target, the estimated error, signal processing noise, and the nominal optical intensity on system performance are discussed.

INDEX TERMS Visible light communications, secrecy capacity, harvested energy, light power transfer.

I. INTRODUCTION

As an efficient supplement to conventional radio frequency (RF) wireless communications, the indoor visible light communications (VLC) has been receiving increasing attention recently, especially in the fields of channel modeling [1], modulation [2], coding [3], positioning [4], performance analysis [5], and transceiver design [6]. VLC is a very promising technology that simultaneously satisfies the illumination and communication requirements in an indoor environment. It has the advantages of having no electromagnetic spectrum regulation and being harmless to human body, and will play a crucial role in the future fifth generation (5G) wireless communications.

In indoor VLC network, many mobile terminals are energy-limited (e.g., sensor nodes for monitoring temperature

The associate editor coordinating the review of this manuscript and approving it for publication was Hayder Al-Hraishawi.

and humidity), which are typically powered by batteries. To prolong the network lifetime, it is necessary to recharge the batteries in time, which incurs very high costs to do this tedious work. A good solution is to harvest energy from the environment to charge these terminals [7], [8]. Recently, simultaneous wireless information and power transfer (SWIPT) has become a new research area, which employs the same emitted signal to transfer both energy and information [9]. Up to now, many SWIPT systems have been developed for RF wireless communication applications, where the ambient RF signals can be used as the sources for energy hunting [10]–[12]. As is well known, the emitted visible-light signals in VLC can also be utilized for energy harvesting. However, few research has discussed the SWIPT in indoor VLC. For indoor VLC, it has a natural advantage to harvest light energy, because the emitted light of the light-emitting diodes (LEDs) can be effectively used by the users. In [13], a sum rate maximizing problem for indoor VLC with SWIPT is investigated. In [14], the optimal design of a dual hop VLC-RF communication system is investigated in terms of date rate maximization. By maximizing the sum rate of VLC, an optimal energy scheduling algorithm is proposed in [15]. To expedite the energy harvesting, increasing transmit power is a simple but efficient approach. However, when the energy receivers are malicious, it has a high potential for them to eavesdrop the information. Therefore, the secure transmission problems arise in VLC systems with SWIPT, which are important to tackle.

To guarantee the information-theoretic security, the physical-layer (PHY) security in VLC has been proposed recently. In [16], the secrecy capacity for the single input single output (SISO) VLC is analyzed. For multiuser VLC, the secrecy outage probability (SOP) and the ergodic secrecy rate (ESR) are derived in [17]. To improve the PHY security, a channel determined subcarrier shifting scheme is proposed in [18] for orthogonal frequency division multiplexing (OFDM) based VLC. In [19], a chaos based PHY security method is introduced for the OFDM based VLC systems with the capacity against known/chosen plaintext attacks. In [20]–[22], the optimal beamforming and robust beamforming schemes are proposed for secure VLC. Note that the above literature only considers the secure information transmission, but the possibility of harvesting energy for VLC is not discussed.

To construct a secure and high-energy-efficient VLC network, it is necessary to combine the PHY security with SWIPT. Therefore, the functionalities of indoor VLC becomes threefold, i.e., illumination, secure information transmission, and light power transfer. In [23], the SOP of a hybrid VLC-RF communication system with energy harvesting is analyzed. For the security and high-energy-efficient VLC network, it is necessary and interesting to analyze the relationship between the harvested energy (HE) and the secrecy capacity (SC), which is often a counter-balance problem. To the best of our knowledge, the SC-HE region for indoor VLC has not been investigated yet.

In this paper, we consider the three-fold functionalities of VLC (i.e., illumination, secure information transmission and light power transfer) and investigate the tradeoff between the SC and the HE. The system includes a transmitter (i.e., Alice), a legitimate receiver (i.e., Bob), and an eavesdropper (i.e., Eve), where Bob can perform SWIPT and Eve can only eavesdrop the information passively. The main contributions of the paper are listed as follows:

- For the indoor VLC system with the non-negative and dimmable average optical intensity constraints, the theoretical expressions of the average HE at Bob and the lower bound of average SC are derived, which are both in closed-forms.
- By employing the dynamic power splitting (DPS), time switching (TS), static power splitting (SPS) and on-off power splitting (OPS) receivers at Bob, the SC-HE regions for the indoor VLC are derived, respectively.
- As a benchmark, the performance upper bound of the SC-HE region is derived for any practical receiver, which is shown to be a rectangular region. For any practical receiver, the derived SC-HE region must be located within the rectangular region.

The rest of the paper is organized as follows. Section II shows the system model. In Section III, the HE and the SC are analyzed. In Section IV, the SC-HE regions are analyzed for different receivers. In Section V, the performance upper bound is analyzed. Numerical results are presented in Section VI, while Section VII concludes the paper.

II. SYSTEM MODEL

As illustrated in Fig. 1, we consider a downlink VLC system, which includes a transmitter employing an LED (i.e., Alice), a legitimate receiver employing a photodiode (PD) (i.e., Bob), and an eavesdropper employing a PD (i.e., Eve). At Bob, the SWIPT is performed. That is, Bob can receive the information from Alice, and can also harvest energy from the light emitted by Alice [23]. Without loss of generality, a DPS receiver is employed to coordinate the information decoding and the energy harvesting [24], as shown in Fig. 2. For Eve,

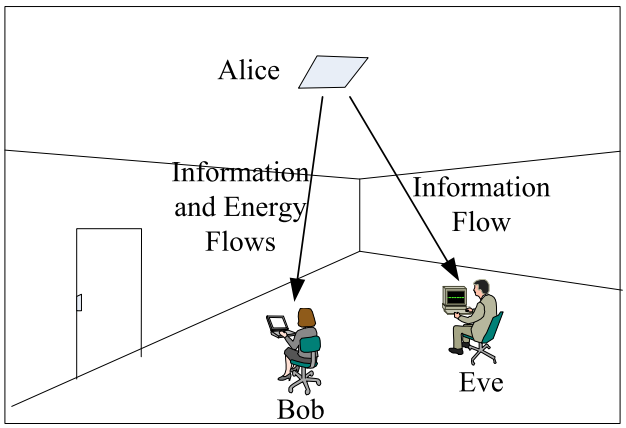

FIGURE 1. A SWIPT based VLC system.

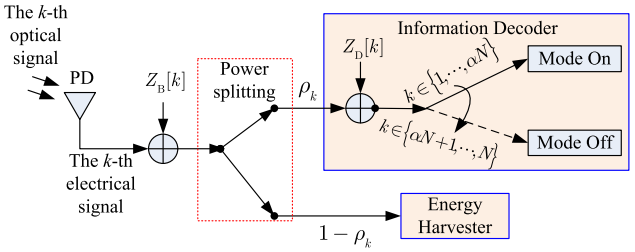

FIGURE 2. Dynamic power splitting receiver at Bob.

it is just an information eavesdropping receiver and cannot harvest energy. That is, when Alice transmits information to Bob, the signal may be overheard by Eve [23].

In the system, we consider a block-transmission with N symbols, each symbol is with a period T_s. For the k-th symbol, the power at Bob is split into two parts, one is used for information decoding with a power ratio ρ_k, $0 \le \rho_k \le 1$, and the other used is for energy harvesting with a ratio $1-\rho_k$, as shown in Fig. 2. For the information receiver at Bob, two modes are employed: Mode on and Mode off. Assume that the first $\lfloor \alpha N \rfloor$ symbols with $k = 1, 2, \cdots, \lfloor \alpha N \rfloor$ operate in Mode on, and the rest symbols with $k = \lfloor \alpha N \rfloor + 1, \cdots, N$ operate in Mode off, where $\alpha \in [0, 1]$ denotes the percentage of time that the information receiver operates in Mode on. To facilitate the description, $\lfloor \alpha N \rfloor$ is assumed to be a positive integer, i.e., $\lfloor \alpha N \rfloor = \alpha N$ always holds. Moreover, in Fig. 2, $Z_B[k] \sim N(0, \sigma_B^2)$ denotes the additive white Gaussian noise (AWGN) at Bob, and σ_B^2 is the noise variance at Bob. $Z_D[k] \sim N(0, \sigma_D^2)$ denotes the signal processing noise for information decoding at Bob, σ_D^2 is the signal processing noise variance at Bob.

For the k-th symbol transmitted by Alice, the received signals at Bob and Eve are given, respectively, by [25]

$$\begin{cases} Y_B[k] = \rho_k \left(H_B X[k] + Z_B[k]\right) + Z_D[k] \\ Y_E[k] = H_E X[k] + Z_E[k] \end{cases} \tag{1}$$

where $Y_B[k]$ and $Y_E[k]$ are the k-th received symbols at Bob and Eve; $X[k]$ is the k-th transmitted optical signal; H_B and H_E denote channel gains for the main channel and the eavesdropping channel, respectively; $Z_E[k] \sim N(0, \sigma_E^2)$ stands for the AWGN at Eve, where σ_E^2 denotes the noise variance at Eve.

In (1), $X[k]$ is the optical intensity of the transmit signal, which should be non-negative, and thus we have [26]

$$X[k] \ge 0 \tag{2}$$

Moreover, considering the dimming requirement, the average optical intensity cannot vary with time, but can be changed with the dimming target. Therefore, the dimmable average optical intensity constraint for indoor VLC is given by [26]

$$\mathbb{E}(X[k]) = \xi P \tag{3}$$

where $\mathbb{E}(\cdot)$ denotes the expect operator, $\xi \in [0, 1]$ represents the dimming target, P denotes the nominal optical intensity of the LED at Alice.

In (1), H_i (i = B or E) denotes the direct current channel gain in VLC. According to [1], such a channel gain is presented as

$$H_i = \frac{(m+1)A}{2\pi D_i^2} T_o g \cos^m(\varphi_i) \cos(\psi_i) \text{rect}\left(\frac{\psi_i}{\Psi}\right) \tag{4}$$

where m is the Lambertian emission order; A and Ψ are the physical area and the field of view (FOV) of the PD; T_o is the optical filter gain; g is the concentrator gain of the PD; D_i is the distance between the transceiver; φ_i and ψ_i are the irradiance angle and the incidence angle; rect$(\cdot)$ denotes the rectangular function. Without loss of generality, we assume that both Bob and Eve can be illuminated by the LED, and thus the incidence angle ψ_i cannot exceed the FOV of the PD Ψ, i.e., $0 \le \psi_i \le \Psi$. Therefore, rect (ψ_i/Ψ) in (4) can be removed to facilitate the analysis.

III. HARVESTED ENERGY AND SECRECY CAPACITY ANALYSIS

In this section, the HE of Bob will be analyzed from the aspect of power transfer. Moreover, the SC will be analyzed from the PHY security aspect.

A. THE HARVESTED ENERGY AT BOB

According to (3), the average transmit optimal power of Alice is $\mathbb{E}(X[k]) = \xi P$, and thus the received optical power at Bob for the k-th symbol is given by

$$\begin{aligned} P_r[k] &= H_B \mathbb{E}(X[k]) \\ &= \xi P \frac{(m+1)A}{2\pi D_B^2} T_o g \cos^m(\varphi_B) \cos(\psi_B) \end{aligned} \tag{5}$$

According to (11) in [27], the received RF power at Bob for the k-th symbol is given by

$$P_{RF}[k] = \frac{C_{RF} \xi^2 P^2 \cos^{2m_A}(\varphi_B) \cos^{2m_B}(\psi_B)}{D_B^4} \tag{6}$$

where C_{RF} is the RF power constant. $m_A = -\ln 2 / \ln \cos(\varphi_{A,1/2})$, $m_B = -\ln 2 / \ln \cos(\varphi_{B,1/2})$, $\varphi_{A,1/2}$ and $\varphi_{B,1/2}$ are semi-angles at half power of Alice and Bob, respectively.

Different from [23], the receiver plane at Bob in this paper is not necessarily perpendicular to the incidence line. Moreover, the imperfect positional information of Bob is also considered. Therefore, (6) can be rewritten as [23]

$$P_{RF}[k] = \frac{C_{RF} \xi^2 P^2 \cos^{2m_A}(\varphi_B) \cos^{2m_B}(\psi'_B)}{D_B^4} \tag{7}$$

where $\psi'_B = \psi_B + \psi_\Delta$, ψ_Δ is the estimated error of ψ_B when the positional information of Bob is imperfect.

For the k-th received symbol, the harvested energy is expressed as

$$E_E^{DPS}[k] = \frac{C_{RF} \xi^2 P^2 \cos^{2m_A}(\varphi_B) \cos^{2m_B}(\psi'_B) T_s \eta (1-\rho_k)}{D_B^4} \tag{8}$$

where $\eta \in (0, 1)$ is the energy harvesting efficiency.

Finally, for all symbols, the average harvested energy at Bob is given by

$$E_{\mathrm{E}}^{\mathrm{DPS}} = \frac{1}{N}\sum_{k=1}^{N}\frac{C_{\mathrm{RF}}\xi^2P^2\cos^{2m_{\mathrm{A}}}(\varphi_{\mathrm{B}})\cos^{2m_{\mathrm{B}}}(\psi'_{\mathrm{B}})T_s\eta(1-\rho_k)}{D_{\mathrm{B}}^4} = \frac{C_{\mathrm{RF}}\xi^2P^2\cos^{2m_{\mathrm{A}}}(\varphi_{\mathrm{B}})\cos^{2m_{\mathrm{B}}}(\psi'_{\mathrm{B}})T_s\eta}{D_{\mathrm{B}}^4} \times\left(1-\frac{1}{N}\sum_{k=1}^{N}\rho_k\right) \tag{9}$$

B. SECRECY CAPACITY

The SC is a key performance indicator to evaluate the PHY security. Due to the constraints of the visible-light signal, the derived SC results in RF wireless communication are not directly applicable to VLC.

For the k-th symbol, the instantaneous SC for the channel (1) with constraints (2) and (3) can be expressed as

$$C_{\mathrm{S}}[k] = \left\{\max_{f_{X[k]}(x)}\left[I(X[k];Y_{\mathrm{B}}[k]) - I(X[k];Y_{\mathrm{E}}[k])\right]\right\}^+ \quad \text{s.t.} \int_0^\infty f_{X[k]}(x)\mathrm{d}x = 1, \quad \int_0^\infty x f_{X[k]}(x)\mathrm{d}x = \xi P \tag{10}$$

where $\{a\}^+ = \max\{a, 0\}$, $I(\cdot;\cdot)$ denotes the mutual information, $f_{X[k]}(x)$ denotes the input distribution of $X[k]$. In (10), it is very hard or even impossible to obtain a closed-form expression for the SC $C_{\mathrm{S}}[k]$. Alternatively, a lower bound on the SC is analyzed in this subsection.

According to [20], for any two functions $f_1(x)$ and $f_2(x)$, we have

$$\max_x\left[f_1(x) - f_2(x)\right] \geq \max_x f_1(x) - \max_x f_2(x) \tag{11}$$

Therefore, the instantaneous SC in (10) is lower-bounded by

$$C_{\mathrm{S}}[k] \geq \left\{\max_{f_{X[k]}(x)} I\left(X[k];Y_{\mathrm{B}}[k]\right) - \max_{f_X[k](x)} I\left(X[k];Y_{\mathrm{E}}[k]\right)\right\}^+ \triangleq \{C_{\mathrm{B}}[k] - C_{\mathrm{E}}[k]\}^+ \tag{12}$$

In this paper, all entropies and conditional entropies are in nats, and thus natural logarithms are employed in the following derivation. According to [29], a lower bound of $C_{\mathrm{B}}[k]$ can be expressed as

$$C_{\mathrm{B}}[k] \geq \frac{1}{2}\ln\left[1+\frac{e\xi^2P^2\rho_k^2H_{\mathrm{B}}^2}{2\pi(\rho_k^2\sigma_{\mathrm{B}}^2+\sigma_{\mathrm{D}}^2)}\right] \tag{13}$$

According to [29], an upper bound of $C_{\mathrm{E}}[k]$ can be presented as

$$C_{\mathrm{E}}[k] \leq \ln\left[\beta e^{-\frac{\delta^2}{2\sigma_{\mathrm{E}}^2}} + \sqrt{2\pi}\sigma_{\mathrm{E}}\mathcal{Q}\left(\frac{\delta}{\sigma_{\mathrm{E}}}\right)\right] + \frac{1}{2}\mathcal{Q}\left(\frac{\delta}{\sigma_{\mathrm{E}}}\right) + \frac{\delta}{2\sqrt{2\pi}\sigma_{\mathrm{E}}}e^{-\frac{\delta^2}{2\sigma_{\mathrm{E}}^2}} + \frac{\delta^2}{2\sigma_{\mathrm{E}}^2}\mathcal{Q}\left(-\frac{\delta+H_{\mathrm{E}}\xi P}{\sigma_{\mathrm{E}}}\right) + \frac{\delta+H_{\mathrm{E}}\xi P}{\beta} + \frac{\sigma_{\mathrm{E}}}{\sqrt{2\pi}\beta}e^{-\frac{\delta^2}{2\sigma_{\mathrm{E}}^2}} - \frac{1}{2}\ln\left(2\pi e\sigma_{\mathrm{E}}^2\right) \tag{14}$$

where $\mathcal{Q}(x) = \int_x^\infty e^{-t^2/2}\mathrm{d}t/\sqrt{2\pi}$ is the Gaussian Q-function, β is chosen by (15), as shown at the bottom of this page, and δ is chosen by

$$\delta = \sigma_{\mathrm{E}}\ln\left(1+\frac{H_{\mathrm{E}}\xi P}{\sigma_{\mathrm{E}}}\right) \tag{16}$$

Substituting (13) and (14) into (12), a lower bound of the instantaneous SC is obtained as

$$C_{\mathrm{L}}^{\mathrm{DPS}}[k] = \left\{\frac{1}{2}\ln\left[1+\frac{e\xi^2P^2\rho_k^2H_{\mathrm{B}}^2}{2\pi(\rho_k^2\sigma_{\mathrm{B}}^2+\sigma_{\mathrm{D}}^2)}\right] - \ln\left[\beta e^{\frac{-\delta^2}{2\sigma_{\mathrm{E}}^2}} + \sqrt{2\pi}\sigma_{\mathrm{E}}\mathcal{Q}\left(\frac{\delta}{\sigma_{\mathrm{E}}}\right)\right] - \frac{1}{2}\mathcal{Q}\left(\frac{\delta}{\sigma_{\mathrm{E}}}\right) - \frac{\delta}{2\sqrt{2\pi}\sigma_{\mathrm{E}}}e^{\frac{-\delta^2}{2\sigma_{\mathrm{E}}^2}} - \frac{\delta^2}{2\sigma_{\mathrm{E}}^2}\mathcal{Q}\left(-\frac{\delta+H_{\mathrm{E}}\xi P}{\sigma_{\mathrm{E}}}\right) - \frac{\delta+H_{\mathrm{E}}\xi P}{\beta} - \frac{\sigma_{\mathrm{E}}}{\sqrt{2\pi}\beta}e^{-\frac{\delta^2}{2\sigma_{\mathrm{E}}^2}} + \frac{1}{2}\ln\left(2\pi e\sigma_{\mathrm{E}}^2\right)\right\}^+ \tag{17}$$

Considering all symbols, the lower bound of average SC is given by

$$C_{\mathrm{L}}^{\mathrm{DPS}} = \frac{1}{N}\sum_{k=1}^{N}C_{\mathrm{L}}^{\mathrm{DPS}}[k] = \frac{1}{N}\sum_{k=1}^{N}\left\{\frac{1}{2}\ln\left[1+\frac{e\xi^2P^2\rho_k^2H_{\mathrm{B}}^2}{2\pi(\rho_k^2\sigma_{\mathrm{B}}^2+\sigma_{\mathrm{D}}^2)}\right] - \ln\left[\beta e^{\frac{-\delta^2}{2\sigma_{\mathrm{E}}^2}} + \sqrt{2\pi}\sigma_{\mathrm{E}}\mathcal{Q}\left(\frac{\delta}{\sigma_{\mathrm{E}}}\right)\right] - \frac{1}{2}\mathcal{Q}\left(\frac{\delta}{\sigma_{\mathrm{E}}}\right) - \frac{\delta}{2\sqrt{2\pi}\sigma_{\mathrm{E}}}e^{\frac{-\delta^2}{2\sigma_{\mathrm{E}}^2}}\right.$$

$$\beta = \frac{1}{2}\left(\delta+H_{\mathrm{E}}\xi P+\frac{\sigma_{\mathrm{E}}}{\sqrt{2\pi}}e^{-\frac{\delta^2}{2\sigma_{\mathrm{E}}^2}}\right) + \frac{1}{2}\sqrt{\left(\delta+H_{\mathrm{E}}\xi P+\frac{\sigma_{\mathrm{E}}}{\sqrt{2\pi}}e^{-\frac{\delta^2}{2\sigma_{\mathrm{E}}^2}}\right)^2 + 4\left(\delta+H_{\mathrm{E}}\xi P+\frac{\sigma_{\mathrm{E}}}{\sqrt{2\pi}}e^{-\frac{\delta^2}{2\sigma_{\mathrm{E}}^2}}\right)\sqrt{2\pi}\sigma_{\mathrm{E}}e^{\frac{\delta^2}{2\sigma_{\mathrm{E}}^2}}\mathcal{Q}\left(\frac{\delta}{\sigma_{\mathrm{E}}}\right)} \tag{15}$$

$$-\frac{\delta^2}{2\sigma_{\mathrm{E}}^2}\mathcal{Q}\left(-\frac{\delta+H_{\mathrm{E}}\xi P}{\sigma_{\mathrm{E}}}\right)-\frac{\delta+H_{\mathrm{E}}\xi P}{\beta}$$
$$-\frac{\sigma_{\mathrm{E}}}{\sqrt{2\pi}\beta}e^{-\frac{\delta^2}{2\sigma_{\mathrm{E}}^2}}+\frac{1}{2}\ln\left(2\pi e\sigma_{\mathrm{E}}^2\right)\Bigg\}^{+} \quad (18)$$

IV. SECRECY CAPACITY-HARVESTED ENERGY REGION FOR DIFFERENT RECEIVERS

In the above section, the theoretical expressions of the HE and the SC are derived. However, the relationship between them has always been considered to be a counter-balance problem. In this section, the SC-HE region is proposed to characterize both the SC (in nat/transmission for secure information transfer) and the HE (in joule for power transfer) pairs.

By using the DPS receiver at Bob, the SC-HE region will be analyzed first. Then, the corresponding SC-HE regions for some variants of the DPS receiver (i.e., the TS, SPS, OPS receivers) will also be obtained.

A. WITH DPS RECEIVER AT BOB

According to (9) and (18), the SC-HE region with DPS receiver at Bob is defined as

$$\mathcal{I}_{\mathrm{SC-HE}}^{\mathrm{DPS}}=\bigcup_{\rho=[\rho_1,\cdots,\rho_N]}\left\{(R,Q)|\,R\le C_{\mathrm{L}}^{\mathrm{DPS}},Q\le E_{\mathrm{E}}^{\mathrm{DPS}}\right\} \quad (19)$$

where $\bigcup$ denotes the union of all elements, $E_{\mathrm{E}}^{\mathrm{DPS}}$ and $C_{\mathrm{L}}^{\mathrm{DPS}}$ can be calculated by (9) and (18), respectively.

B. WITH TS RECEIVER AT BOB

The TS receiver at Bob is shown in Fig. 3. In this case, the first αN symbols operate in Mode on, and all signal power is used for information decoding. The rest $(1-\alpha)N$ symbols operate in Mode off, and all signal power is used for energy harvesting. Therefore, ρ_k becomes

$$\rho_k=\begin{cases}1, & \text{if } k=1,2,\cdots,\alpha N\\ 0, & \text{if } k=\alpha N+1,\cdots,N\end{cases} \quad (20)$$

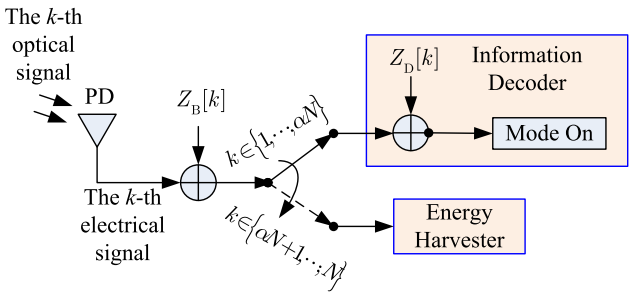

FIGURE 3. The TS receiver at Bob.

In this case, the average HE is given by

$$E_{\mathrm{E}}^{\mathrm{TS}}=\frac{1}{N}\sum_{k=1}^{(1-\alpha)N}\frac{C_{\mathrm{RF}}\xi^2P^2\cos^{2m_{\mathrm{A}}}(\varphi_{\mathrm{B}})\cos^{2m_{\mathrm{B}}}(\psi_{\mathrm{B}}')T_s\eta}{D_{\mathrm{B}}^4}$$
$$=\frac{C_{\mathrm{RF}}\xi^2P^2\cos^{2m_{\mathrm{A}}}(\varphi_{\mathrm{B}})\cos^{2m_{\mathrm{B}}}(\psi_{\mathrm{B}}')T_s\eta(1-\alpha)}{D_{\mathrm{B}}^4} \quad (21)$$

The lower bound of the average SC is expressed as

$$C_{\mathrm{L}}^{\mathrm{TS}}=\frac{1}{N}\sum_{k=1}^{\alpha N}C_{\mathrm{L}}^{DPS}[k](\rho_k=1)$$
$$=\alpha\Bigg\{\frac{1}{2}\ln\left[1+\frac{e\xi^2P^2H_{\mathrm{B}}^2}{2\pi(\sigma_{\mathrm{B}}^2+\sigma_{\mathrm{D}}^2)}\right]$$
$$-\ln\left[\beta e^{\frac{-\delta^2}{2\sigma_{\mathrm{E}}^2}}+\sqrt{2\pi}\sigma_{\mathrm{E}}\mathcal{Q}\left(\frac{\delta}{\sigma_{\mathrm{E}}}\right)\right]-\frac{1}{2}\mathcal{Q}\left(\frac{\delta}{\sigma_{\mathrm{E}}}\right)$$
$$-\frac{\delta}{2\sqrt{2\pi}\sigma_{\mathrm{E}}}e^{-\frac{\delta^2}{2\sigma_{\mathrm{E}}^2}}-\frac{\delta^2}{2\sigma_{\mathrm{E}}^2}\mathcal{Q}\left(-\frac{\delta+H_{\mathrm{E}}\xi P}{\sigma_{\mathrm{E}}}\right)$$
$$-\frac{\delta+H_{\mathrm{E}}\xi P}{\beta}-\frac{\sigma_{\mathrm{E}}}{\sqrt{2\pi}\beta}e^{-\frac{\delta^2}{2\sigma_{\mathrm{E}}^2}}+\frac{1}{2}\ln\left(2\pi e\sigma_{\mathrm{E}}^2\right)\Bigg\}^{+} \quad (22)$$

According to (21) and (22), the SC-HE region with the TS receiver at Bob is given by

$$\mathcal{I}_{\mathrm{SC-HE}}^{\mathrm{TS}}=\bigcup_{\alpha}\left\{(R,Q)|\,R\le C_{\mathrm{L}}^{\mathrm{TS}},Q\le E_{\mathrm{E}}^{\mathrm{TS}}\right\} \quad (23)$$

where $E_{\mathrm{E}}^{\mathrm{TS}}$ and $C_{\mathrm{L}}^{\mathrm{TS}}$ can be calculated by (21) and (22), respectively.

Remark 1: For the TS receiver, the HE in (21) decreases linearly with the increase of α, while the SC in (22) increases linearly with the increase of α. According to this observation, it can be obviously concluded that there is a linear relationship between the SC and the HE for the TS receiver.

C. WITH SPS RECEIVER AT BOB

The SPS receiver at Bob is shown in Fig. 4. For this receiver, the information receiver at Bob operates in Mode on for all symbols $k=1,\cdots,N$. Moreover, ρ_k becomes

$$\rho_k=\rho,\quad k=1,\cdots,N \quad (24)$$

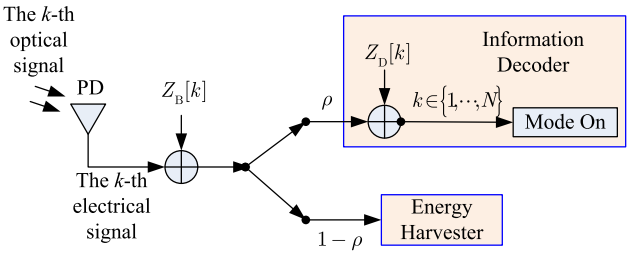

FIGURE 4. The SPS receiver at Bob.

In this case, the average HE is given by

$$E_{\mathrm{E}}^{\mathrm{SPS}}=\frac{1}{N}\sum_{k=1}^{N}\frac{C_{\mathrm{RF}}\xi^2P^2\cos^{2m_{\mathrm{A}}}(\varphi_{\mathrm{B}})\cos^{2m_{\mathrm{B}}}(\psi_{\mathrm{B}}')T_s\eta(1-\rho)}{D_{\mathrm{B}}^4}$$
$$=\frac{C_{\mathrm{RF}}\xi^2P^2\cos^{2m_{\mathrm{A}}}(\varphi_{\mathrm{B}})\cos^{2m_{\mathrm{B}}}(\psi_{\mathrm{B}}')T_s\eta(1-\rho)}{D_{\mathrm{B}}^4} \quad (25)$$

Moreover, the lower bound of the average SC can be expressed as

$$C_{\mathrm{L}}^{\mathrm{SPS}} = \left\{ \frac{1}{2}\ln\left[1+\frac{e\xi^2P^2\rho^2H_{\mathrm{B}}^2}{2\pi(\rho^2\sigma_{\mathrm{B}}^2+\sigma_{\mathrm{D}}^2)}\right] - \ln\left[\beta e^{\frac{-\delta^2}{2\sigma_{\mathrm{E}}^2}} + \sqrt{2\pi}\sigma_{\mathrm{E}}\mathcal{Q}\left(\frac{\delta}{\sigma_{\mathrm{E}}}\right)\right] - \frac{1}{2}\mathcal{Q}\left(\frac{\delta}{\sigma_{\mathrm{E}}}\right) - \frac{\delta}{2\sqrt{2\pi}\sigma_{\mathrm{E}}}e^{-\frac{\delta^2}{2\sigma_{\mathrm{E}}^2}} - \frac{\delta^2}{2\sigma_{\mathrm{E}}^2}\mathcal{Q}\left(-\frac{\delta+H_{\mathrm{E}}\xi P}{\sigma_{\mathrm{E}}}\right) - \frac{\delta+H_{\mathrm{E}}\xi P}{\beta} - \frac{\sigma_{\mathrm{E}}}{\sqrt{2\pi}\beta}e^{-\frac{\delta^2}{2\sigma_{\mathrm{E}}^2}} + \frac{1}{2}\ln\left(2\pi e\sigma_{\mathrm{E}}^2\right)\right\}^+ \tag{26}$$

Therefore, the SC-HE region with SPS receiver at Bob is given by

$$\mathcal{I}_{\mathrm{SC-HE}}^{\mathrm{SPS}} = \bigcup_{\rho}\left\{(R,Q)|\, R\le C_{\mathrm{L}}^{\mathrm{SPS}}, Q\le E_{\mathrm{E}}^{\mathrm{SPS}}\right\} \tag{27}$$

where $E_{\mathrm{E}}^{\mathrm{SPS}}$ and $C_{\mathrm{L}}^{\mathrm{SPS}}$ are determined by (25) and (26), respectively.

Remark 2: For the SPS receiver, the HE in (25) decreases linearly with the increase of ρ, however, the SC in (26) does not increase linearly with the increase of ρ. Therefore, unlike *Remark 1*, the relationship between the SC and the HE for SPS receiver is nonlinear.

Remark 3: The SC-HE region with SPS receiver at Bob is the same as that with the DPS receiver at Bob, i.e., $\mathcal{I}_{\mathrm{SC-HE}}^{\mathrm{DPS}} = \mathcal{I}_{\mathrm{SC-HE}}^{\mathrm{SPS}}$.

Proof 1: See [24, Proposition 4.1].

From *Remark 3*, it can be known that, for the block-transmission with N symbols, the SC-HE region for the SPS receiver with fixed power splitting ratio is the same as that for the DPS receiver with adjustable power splitting ratio. Therefore, compared to the DPS receiver, the SPS receiver is a better choice in practice from the viewpoint of complexity.

Remark 4: From (21) and (25), it can be seen that the HE of the TS receiver is the same as that of the SPS receiver when $\alpha = \rho = c$. Moreover, the smaller the parameter c is, the larger the HE becomes. Referring to (22) and (26), when $c = 0$ (i.e., the HE achieves its maximum value) and $c = 1$ (i.e., the HE is zero), the SC for the TS receiver is the same as that of the SPS receiver.

D. WITH OPS RECEIVER AT BOB

The OPS receiver at Bob is shown in Fig. 5. For this receiver, all signal power for the first αN symbols is used for information decoding. For the rest symbols, the power ratio of decoding information and harvesting energy is set to be a constant ρ. Therefore, we have

$$\rho_k = \begin{cases} 1, & k = 1,\cdots,\alpha N \\ \rho, & k = \alpha N+1,\cdots,N \end{cases} \tag{28}$$

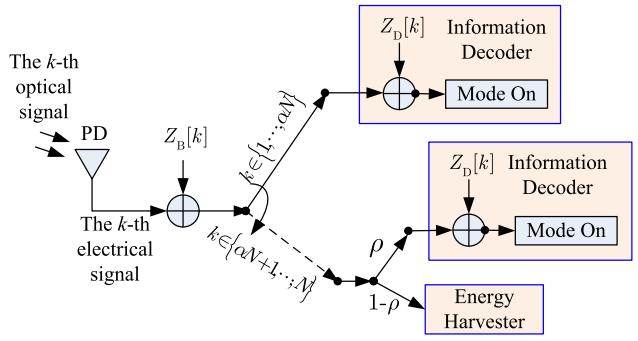

FIGURE 5. The OPS receiver at Bob.

In this case, the average HE is given by

$$E_{\mathrm{E}}^{\mathrm{OPS}} = \frac{1}{N}\sum_{k=\alpha N+1}^{N}\frac{C_{\mathrm{RF}}\xi^2P^2\cos^{2m_{\mathrm{A}}}(\varphi_{\mathrm{B}})\cos^{2m_{\mathrm{B}}}(\psi_{\mathrm{B}}')T_s\eta(1-\rho)}{D_{\mathrm{B}}^4} = \frac{C_{\mathrm{RF}}\xi^2P^2\cos^{2m_{\mathrm{A}}}(\varphi_{\mathrm{B}})\cos^{2m_{\mathrm{B}}}(\psi_{\mathrm{B}}')T_s\eta(1-\rho)(1-\alpha)}{D_{\mathrm{B}}^4} \tag{29}$$

The lower bound of the average SC is expressed as

$$C_{\mathrm{L}}^{\mathrm{OPS}} = C_{\mathrm{L}}^{\mathrm{TS}} + (1-\alpha)C_{\mathrm{L}}^{\mathrm{SPS}} \tag{30}$$

Therefore, the SC-HE region with OPS receiver at Bob is given by

$$\mathcal{I}_{\mathrm{SC-HE}}^{\mathrm{OPS}} = \bigcup_{\rho,\alpha}\left\{(R,Q)|\, R\le C_{\mathrm{L}}^{\mathrm{OPS}}, Q\le E_{\mathrm{E}}^{\mathrm{OPS}}\right\} \tag{31}$$

where $E_{\mathrm{E}}^{\mathrm{OPS}}$ and $C_{\mathrm{L}}^{\mathrm{OPS}}$ are determined by (29) and (30), respectively.

Remark 5: When $\alpha = 0$, $C_{\mathrm{L}}^{\mathrm{TS}}$ in (30) becomes zero, and thus the SC-HE region with OPS receiver at Bob reduces to that with SPS receiver at Bob, i.e., $\mathcal{I}_{\mathrm{SC-HE}}^{\mathrm{OPS}}(\alpha=0) = \mathcal{I}_{\mathrm{SC-HE}}^{\mathrm{SPS}}$.

Remark 6: When $\rho = 0$, $C_{\mathrm{L}}^{\mathrm{SPS}}$ in (30) becomes zero, and thus the SC-HE region with OPS receiver at Bob reduces to that with TS receiver at Bob, i.e., $\mathcal{I}_{\mathrm{SC-HE}}^{\mathrm{OPS}}(\rho=0) = \mathcal{I}_{\mathrm{SC-HE}}^{\mathrm{TS}}$.

Remark 7: According to *Remark 5* and *Remark 6*, it can be concluded that the system with OPS receiver at Bob is better than or equivalent that with TS or SPS receiver at Bob.

V. PERFORMANCE UPPER BOUND FOR ANY PRACTICAL RECEIVER

In Section IV, the SC-HE regions are analyzed for the DPS, TS, SPS and OPS receivers at Bob, respectively. As can be seen obviously, the SC-HE region varies for different kinds of receivers. In this section, a performance upper bound of the SC-HE region will be provided, which is suitable for any practical receiver.

For energy harvesting, the maximum HE cannot exceed the received energy. Therefore, the maximum HE is given by

$$E_{\mathrm{E}}^{\mathrm{Upp}} = \frac{C_{\mathrm{RF}}\xi^2 P^2 \cos^{2m_{\mathrm{A}}}(\varphi_{\mathrm{B}})\cos^{2m_{\mathrm{B}}}(\psi'_{\mathrm{B}})T_s}{D_{\mathrm{B}}^4} \tag{32}$$

Note that the upper bound (32) cannot be achieved unless the energy harvesting efficiency η is made ideally equal to one.

For information decoding, by using the data processing inequality, the maximum SC is upper-bounded by

$$\begin{aligned} C_{\mathrm{L}}^{\mathrm{Upp}} = \Bigg\{ & \frac{1}{2}\ln\left[1+\frac{e\xi^2P^2H_{\mathrm{B}}^2}{2\pi\sigma_{\mathrm{B}}^2}\right] \\ & - \ln\left[\beta e^{\frac{-\delta^2}{2\sigma_{\mathrm{E}}^2}} + \sqrt{2\pi}\sigma_{\mathrm{E}}\mathcal{Q}\left(\frac{\delta}{\sigma_{\mathrm{E}}}\right)\right] - \frac{1}{2}\mathcal{Q}\left(\frac{\delta}{\sigma_{\mathrm{E}}}\right) \\ & - \frac{\delta}{2\sqrt{2\pi}\sigma_{\mathrm{E}}}e^{-\frac{\delta^2}{2\sigma_{\mathrm{E}}^2}} - \frac{\delta^2}{2\sigma_{\mathrm{E}}^2}\mathcal{Q}\left(-\frac{\delta+H_{\mathrm{E}}\xi P}{\sigma_{\mathrm{E}}}\right) \\ & - \frac{\delta+H_{\mathrm{E}}\xi P}{\beta} - \frac{\sigma_{\mathrm{E}}}{\sqrt{2\pi}\beta}e^{-\frac{\delta^2}{2\sigma_{\mathrm{E}}^2}} + \frac{1}{2}\ln\left(2\pi e\sigma_{\mathrm{E}}^2\right)\Bigg\}^+ \end{aligned} \tag{33}$$

Note that the upper bound (33) cannot be achieved because of the existence of the additional processing noise Z_{D}.

Based on (32) and (33), the upper bound of the SC-HE region can be written as

$$\mathcal{I}_{\mathrm{SC-HE}}^{\mathrm{Upp}} = \left\{(R,Q)|\, R \le C_{\mathrm{L}}^{\mathrm{Upp}}, Q \le E_{\mathrm{E}}^{\mathrm{Upp}}\right\} \tag{34}$$

Note that the region in (34) is a rectangular, which is consisted by the four vertices (0,0), $(C_{\mathrm{L}}^{\mathrm{Upp}}, 0)$, $(0, E_{\mathrm{E}}^{\mathrm{Upp}})$ and $(C_{\mathrm{L}}^{\mathrm{Upp}}, E_{\mathrm{E}}^{\mathrm{Upp}})$. The rectangular region in (34) is valid for any practical receiver.

VI. NUMERICAL RESULTS

In this section, an indoor VLC system with Alice, Bob and Eve is considered. The positions of Alice, and Bob are set to be (2.5m, 2.5m, 3m) and (2m, 2m, 0.8m), and the position of Eve is set to be (a, b, c), which varies with the considered scenario. Numerical results will be provided to show the SC-HE regions under different scenarios. Note that all numerical results are obtained by using MATLAB. To facilitate the simulation, the noise variances of Bob and Eve are set to be one. The other simulation parameters are provided in Table 1.

TABLE 1. Main simulation parameters.

Parameters	Symbols	Values
Number of symbols per block	N	20
Symbol period	T_s	1s
RF power constant	C_{RF}	7.8×10^{-3}
Semi-angle at half power of Alice	$\varphi_{\mathrm{A},1/2}$	50^0
Semi-angle at half power of Bob	$\varphi_{\mathrm{B},1/2}$	22^0
Energy harvesting efficiency	η	0.9
Incidence angle of PD	$\psi_{\mathrm{B}}, \psi_{\mathrm{E}}$	0^0

Fig. 6 shows the SC-HE regions for different receivers at Bob and different dimming targets ξ when $\sigma_{\mathrm{D}} = 1$, $\psi_\Delta = 2^0$, $P = 20$ dB and $(a, b, c) = (0.2\text{ m}, 0.5\text{ m}, 0.8\text{ m})$. As can be seen, the system with the OPS receiver always achieves the best performance. This conclusion coincides with that in *Remark 7*. The system with the DPS receiver gets the same performance as the system with the SPS receiver, which verifies the conclusion in *Remark 3*. When the HE achieves its maximum and minimum values, the same SC performance can be obtained for the TS and DPS/SPS receivers, which verifies *Remark 4*. As can be seen, the SC-HE curve for the TS receiver is linear, which coincides with *Remark 1*, while the SC-HE curve for the DPS/SPS receiver is nonlinear as shown in *Remark 2*. Furthermore, the TS receiver achieves the worst SC when the HE at Bob is small. On the contrary, the TS receiver obtains the best SC when the HE at Bob is large. Moreover, with the increase of ξ, the SC-HE region enlarges, which indicates that the system performance improves. Even so, all SC-HE regions cannot exceed the performance upper bound.

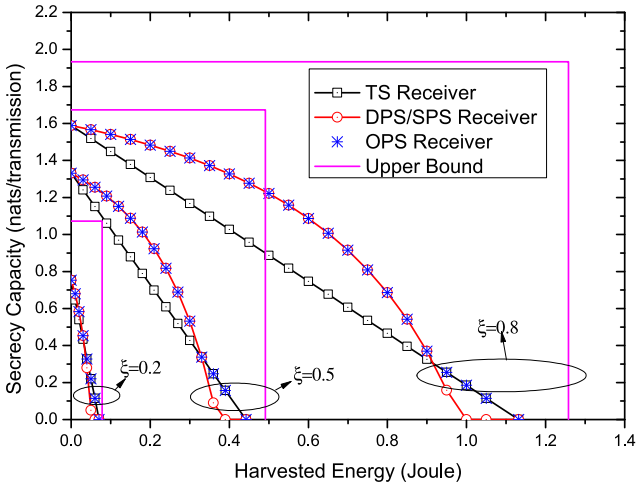

FIGURE 6. The SC-HE regions for different receivers at Bob and different ξ when $\sigma_{\mathrm{D}} = 1$, $\psi_\Delta = 2^0$, $P = 20$ dB and $(a, b, c) = (0.2\text{ m}, 0.5\text{ m}, 0.8\text{ m})$.

Fig. 7 depicts the SC-HE regions for different receivers at Bob and different estimated errors ψ_Δ when $\sigma_{\mathrm{D}} = 1, \xi = 0.8$, $P = 20$ dB and $(a, b, c) = (0.2\text{ m}, 0.5\text{ m}, 0.8\text{ m})$. Similar to Fig. 6, the OPS receiver is the best receiver; the DPS receiver and the SPS receiver achieve the same performance; the TS receiver is the worst one for small HE at Bob, and vice versa. Moreover, when $\psi_\Delta = 0^0$, the estimation of ψ_{B} is perfect, the SC-HE region is the largest. As can be seen, with the increase of ψ_Δ, the SC-HE region becomes smaller and smaller. This indicates that the larger the estimated error, the worse the performance becomes.

Fig. 8 shows the SC-HE regions for different receivers at Bob and different signal processing noise standard variances σ_{D} when $\psi_\Delta = 2^0$, $P = 20$ dB, $\xi = 0.8$ and $(a, b, c) = (0.2\text{ m}, 0.5\text{ m}, 0.8\text{ m})$. It can be observed that the SC-HE region enlarges with the decrease of σ_{D}. In other words, for a fixed HE, the secrecy capacity increases with the decrease of σ_{D}. Different from Fig. 6 and Fig. 7, the performance upper bound in Fig. 8 does not change with σ_{D}. Once again,

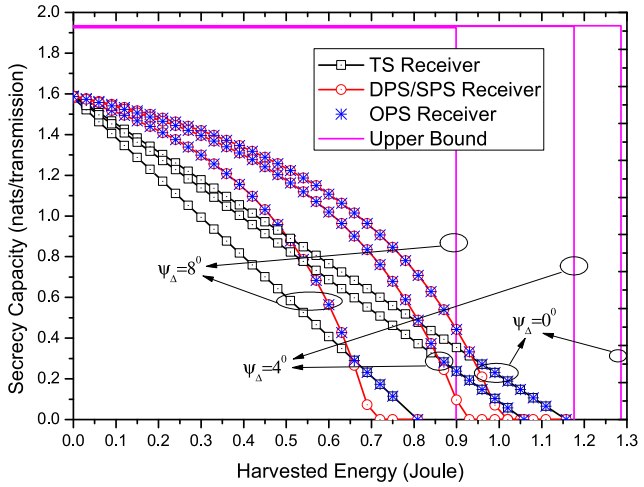

FIGURE 7. The SC-HE regions for different receivers at Bob and different ψ_Δ when $\sigma_D = 1$, $\xi = 0.8$, $P = 20$ dB and $(a, b, c) = (0.2\text{ m}, 0.5\text{ m}, 0.8\text{ m})$.

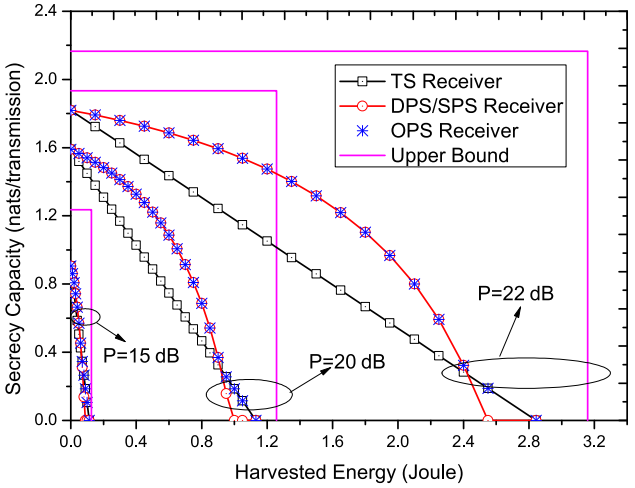

FIGURE 9. The SC-HE regions with different P for different receivers at Bob when $\sigma_D = 1$, $\psi_\Delta = 2^0$, $\xi = 0.8$ and $(a, b, c) = (0.2\text{ m}, 0.5\text{ m}, 0.8\text{ m})$.

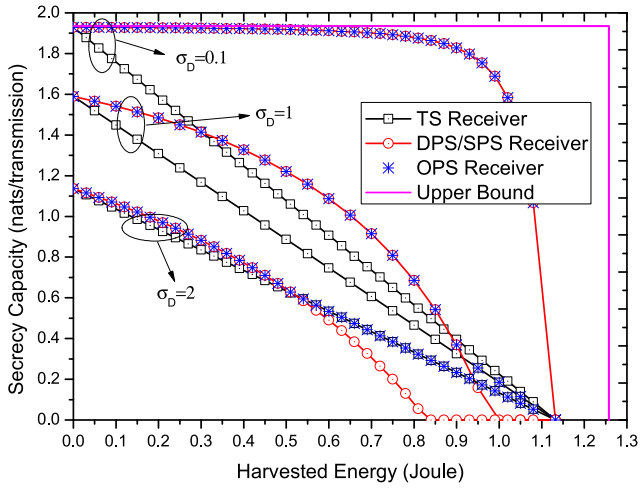

FIGURE 8. The SC-HE regions for different receivers at Bob and different σ_D when $\psi_\Delta = 2^0$, $P = 20$ dB, $\xi = 0.8$ and $(a, b, c) = (0.2\text{ m}, 0.5\text{ m}, 0.8\text{ m})$.

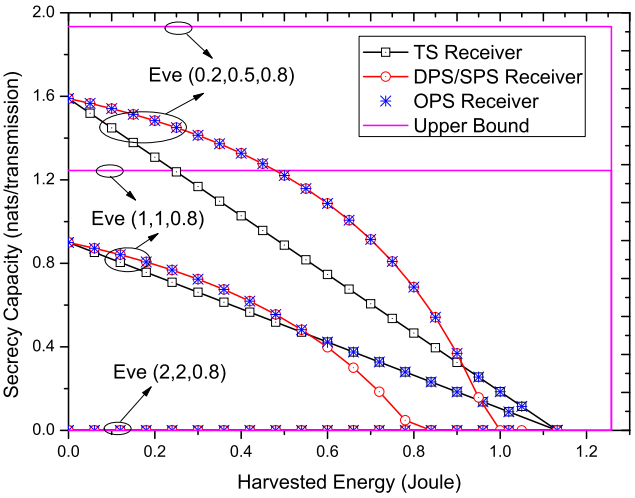

FIGURE 10. The SC-HE regions with different positions of Eve for different receivers at Bob when $\sigma_D = 1$, $\psi_\Delta = 2^0$, $\xi = 0.8$ and $P = 20$ dB.

all SC-HE regions are not exceed the performance upper bound.

Fig. 9 plots the SC-HE regions with different nominal optical intensities P for different receivers at Bob when $\sigma_D = 1$, $\psi_\Delta = 2^0$, $\xi = 0.8$ and $(a, b, c) = (0.2\text{ m}, 0.5\text{ m}, 0.8\text{ m})$. In Fig. 9, the SC-HE region varies with P. Specifically, with the increase of P, both the SC and the HE increase rapidly. That is, large SC-HE region can be obtained by using large P. Moreover, the nominal optical intensity P also has a large impact on the performance upper bound.

Fig. 10 shows the SC-HE regions with different positions of Eve for different receivers at Bob when $\sigma_D = 1$, $\psi_\Delta = 2^0$, $\xi = 0.8$ and $P = 20$ dB. It can be seen that the position of Eve has a strong impact on the SC-HE region. When $(a, b, c) = (0.2\text{ m}, 0.5\text{ m}, 0.8\text{ m})$, the main channel is better than the eavesdropping channel, and thus large SC-HE region can be obtained. When Eve moves from $(0.2\text{ m}, 0.5\text{ m}, 0.8\text{ m})$ to $(1\text{ m}, 1\text{ m}, 0.8\text{ m})$, the quality of eavesdropping channel improves, and thus the SC performance degrades. When Eve moves to $(2\text{ m}, 2\text{ m}, 0.8\text{ m})$, Bob and Eve are located at the same position, the SC becomes zero. Moreover, since the energy is harvested at Bob, the HE performance is not affected by the position of Eve.

VII. CONCLUSIONS

This paper has analyzed the tradeoff between SC and HE and derived the SC-HE regions for different practical receivers. The main conclusions are listed as follows:

1) The SC-HE regions have been obtained for different receivers (i.e., DPS, TS, SPS and OPS receivers). The TS, SPS, and OPS receivers are the variants of the DPS receiver. The OPS receiver always obtains the best performance. The DPS and SPS receivers can achieve the same performance. The TS receiver has good performance when HE is large, and vice versa.

2) For all receivers, with the increase of the dimming target ξ, the SC-HE region enlarges.
3) For all receivers, the estimated error of ψ_B has a negative impact on the system performance.
4) For all receivers, with the increase of the signal processing noise variance σ_D^2, the SC-HE region performance degrades.
5) For all receivers, the larger the nominal optical intensity P is, the better the system performance becomes.
6) For all receivers, the position of Eve has a large impact on SC performance, however, it has no effect on HE performance.

REFERENCES

[1] T. Komine and M. Nakagawa, "Fundamental analysis for visible-light communication system using LED lights," *IEEE Trans. Consum. Electron.*, vol. 50, no. 1, pp. 100–107, Feb. 2004.
[2] J.-Y. Wang, Z. Yang, Y. Wang, and M. Chen, "On the performance of spatial modulation-based optical wireless communications," *IEEE Photon. Technol. Lett.*, vol. 28, no. 19, pp. 2094–2097, Oct. 1, 2016.
[3] S. Kim and S.-Y. Jung, "Novel FEC coding scheme for dimmable visible light communication based on the modified Reed–Müller codes," *IEEE Photon. Technol. Lett.*, vol. 23, no. 20, pp. 1514–1516, Oct. 15, 2011.
[4] B. Zhu, J. Cheng, Y. Wang, J. Yan, and J. Wang, "Three-dimensional VLC positioning based on angle difference of arrival with arbitrary tilting angle of receiver," *IEEE J. Sel. Areas Commun.*, vol. 36, no. 1, pp. 8–22, Jan. 2018.
[5] J.-Y. Wang, J. Dai, R. Guan, L. Jia, Y. Wang, and M. Chen, "Channel capacity and receiver deployment optimization for multi-input multi-output visible light communications," *Opt. Express*, vol. 24, no. 12, pp. 13060–13074, Jun. 2016.
[6] S. Rajbhandari *et al.*, "High-speed integrated visible light communication system: Device constraints and design considerations," *IEEE J. Sel. Areas Commun.*, vol. 33, no. 9, pp. 1750–1757, Sep. 2015.
[7] S. Sudevalayam and P. Kulkarni, "Energy harvesting sensor nodes: Survey and implications," *IEEE Commun. Surveys Tuts.*, vol. 13, no. 3, pp. 443–461, 3rd Quart., 2011.
[8] X. Lu, P. Wang, D. Niyato, D. I. Kim, and Z. Han, "Wireless networks with RF energy harvesting: A contemporary survey," *IEEE Commun. Surveys Tuts.*, vol. 17, no. 2, pp. 757–789, 2nd Quart., 2015.
[9] G. Pan *et al.*, "On secrecy performance of MISO SWIPT systems with TAS and imperfect CSI," *IEEE Trans. Commun.*, vol. 64, no. 9, pp. 3831–3843, Sep. 2016.
[10] R. Zhang and C. K. Ho, "MIMO broadcasting for simultaneous wireless information and power transfer," *IEEE Trans. Wireless Commun.*, vol. 12, no. 5, pp. 1989–2001, May 2013.
[11] M. R. A. Khandaker and K.-K. Wong, "Masked beamforming in the presence of energy-harvesting eavesdroppers," *IEEE Trans. Inf. Forensics Security*, vol. 10, no. 1, pp. 40–54, Jan. 2015.
[12] A. Singh, M. R. Bhatnagar, and R. K. Mallik, "Secrecy outage of a simultaneous wireless information and power transfer cognitive radio system," *IEEE Wireless Commun. Lett.*, vol. 5, no. 3, pp. 288–291, Jun. 2016.
[13] Y. Li, N. Huang, J.-Y. Wang, Z. Yang, and W. Xu, "Sum rate maximization for VLC systems with simultaneous wireless information and power transfer," *IEEE Photon. Technol. Lett.*, vol. 29, no. 6, pp. 531–534, Mar. 15, 2017.
[14] T. Rakia, H.-C. Yang, F. Gebali, and M.-S. Alouini, "Optimal design of dual-hop VLC/RF communication system with energy harvesting," *IEEE Commun. Lett.*, vol. 20, no. 10, pp. 1979–1982, Oct. 2016.
[15] V. Aggarwai, Z. Wang, X. Wang, and M. Ismail, "Energy scheduling for optical channels with energy harvesting devices," *IEEE Trans. Green Commun. Netw.*, vol. 2, no. 1, pp. 154–162, Mar. 2018.
[16] J.-Y. Wang, C. Liu, J.-B. Wang, Y. Wu, M. Lin, and J. Cheng, "Physical-layer security for indoor visible light communications: Secrecy capacity analysis," *IEEE Trans. Commun.*, vol. 66, no. 12, pp. 6423–6436, Dec. 2018.
[17] L. Yin and H. Hass, "Physical-layer security in multiuser visible light communication networks," *IEEE J. Sel. Areas Commun.*, vol. 36, no. 1, pp. 162–174, Jan. 2018.
[18] H. Lu, L. Zhang, W. Chen, and Z. Wu, "Design and analysis of physical layer security based on ill-posed theory for optical OFDM-based VLC system over real-valued visible light channel," *IEEE Photon. J.*, vol. 8, no. 6, Dec. 2016, Art. no. 7805919.
[19] Y. M. Al-Moliki, M. T. Alresheedi, and Y. Al-Harthi, "Physical-layer security against known/chosen plaintext attacks for OFDM-based VLC system," *IEEE Commun. Lett.*, vol. 21, no. 12, pp. 2606–2609, Dec. 2017.
[20] A. Mostafa and L. Lampe, "Physical-layer security for MISO visible light communication channels," *IEEE J. Sel. Areas Commun.*, vol. 33, no. 9, pp. 1806–1818, Sep. 2015.
[21] S. Ma, Z. L. Dong, H. Li, Z. Lu, and S. Li, "Optimal and robust secure beamformer for indoor MISO visible light communication," *J. Lightw. Technol.*, vol. 34, no. 21, pp. 4988–4998, Nov. 1, 2016.
[22] H. Shen, Y. Deng, W. Xu, and C. Zhao, "Secrecy-oriented transmitter optimization for visible light communication systems," *IEEE Photon. J.*, vol. 8, no. 5, Oct. 2016, Art. no. 7905914.
[23] G. Pan, J. Ye, and Z. Ding, "Secure hybrid VLC-RF systems with light energy harvesting," *IEEE Trans. Commun.*, vol. 65, no. 10, pp. 4348–4359, Oct. 2017.
[24] X. Zhou, R. Zhang, and C. K. Ho, "Wireless information and power transfer: Architecture design and rate-energy tradeoff," *IEEE Trans. Commun.*, vol. 61, no. 11, pp. 4754–4767, Nov. 2013.
[25] G. Pan, C. Tang, T. Li, and Y. Chen, "Secrecy performance analysis for SIMO simultaneous wireless information and power transfer systems," *IEEE Trans. Commun.*, vol. 63, no. 9, pp. 3423–3433, Sep. 2015.
[26] J.-B. Wang, Q.-S. Hu, J. Wang, M. Chen, and J.-Y. Wang, "Tight bounds on channel capacity for dimmable visible light communications," *J. Lightw. Technol.*, vol. 31, no. 23, pp. 3771–3779, Dec. 1, 2013.
[27] H.-S. Kim, D.-R. Kim, S.-H. Yang, Y.-H. Son, and S.-K. Han, "An indoor visible light communication positioning system using a RF carrier allocation technique," *J. Lightw. Technol.*, vol. 31, no. 1, pp. 134–144, Jan. 1, 2013.
[28] J.-Y. Wang *et al.*, "Improvement of BER performance by tilting receiver plane for indoor visible light communications with input-dependent noise," in *Proc. IEEE Int. Conf. Commun. (ICC)*, Paris, France, May 2017, pp. 1–6.
[29] A. Lapidoth, S. M. Moser, and M. A. Wigger, "On the capacity of free-space optical intensity channels," *IEEE Trans. Inf. Theory*, vol. 55, no. 10, pp. 4449–4461, Oct. 2009.

JIN-YUAN WANG (S'12–M'16) received the B.S. degree in communication engineering from the College of Information and Electrical Engineering, Shandong University of Science and Technology, Qingdao, China, in 2009, the M.S. degree in electronic and communication engineering from the College of Electronic and Information Engineering, Nanjing University of Aeronautics and Astronautics, Nanjing, China, in 2012, and the Ph.D. degree in information and communication engineering from the National Mobile Communications Research Laboratory, Southeast University, Nanjing, in 2015. He is currently a Lecturer with the Key Lab of Broadband Wireless Communication and Sensor Network Technology, Nanjing University of Posts and Telecommunications, Nanjing. He has authored/co-authored over 90 journal/conference papers. His current research interest includes visible light communications. He has been a Technical Program Committee member for many international conferences, including the IEEE ICC and WTS. He also serves as a Reviewer for many journals.

SHENG-HONG LIN received the B.S. degree in electrical engineering and automation from the Taizhou College, Nanjing Normal University, Taizhou, China, in 2011, and the M.S. degree in power systems and automation from Nanjing Normal University, Nanjing, China, in 2016. She is currently pursuing the Ph.D. degree in information and communication engineering with the Nanjing University of Posts and Telecommunications, Nanjing. Since 2016, she has been a Teaching Assistant with the Nanjing Institute of Mechatronic Technology, China. Her current research interest includes visible light communications.

YU QIU received the B.S. degree in communication engineering from the School of Electronic and Optical Engineering, Nanjing University of Science and Technology, China, in 2017. He is currently pursuing the M.S. degree in communication and information system with the National Mobile Communications Research Laboratory, Southeast University, Nanjing, China. His current research interests include simultaneous wireless information and power transfer, and physical-layer security in visible light communications.

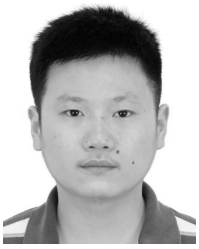

NUO HUANG received the B.S. degree in electronics and information engineering from the Huazhong University of Science and Technology, Wuhan, China, in 2012. He is currently pursuing the Ph.D. degree with the National Mobile Communications Research Laboratory, Southeast University, Nanjing, China. From 2015 to 2017, he was a Visiting Student with the Department of Electrical Engineering, Columbia University, New York, NY, USA. His research interests include resource allocation and transceiver design in optical wireless communications.

JUN-BO WANG (M'11) received the B.S. degree in computer science from the Hefei University of Technology, Hefei, China, in 2003, and the Ph.D. degree in communications engineering from the National Mobile Communications Research Laboratory, Southeast University, Nanjing, China, in 2008, where he is currently an Associate Professor. From 2008 to 2013, he was with the Nanjing University of Aeronautics and Astronautics, China. From 2011 to 2013, he was a Postdoctoral Fellow with the National Laboratory for Information Science and Technology, Tsinghua University, Beijing, China. From 2016 to 2018, he was a Marie Skłodowska-Curie Visiting Scholar with the University of Kent, U.K. His current research interests include wireless communications, signal processing, and information theory and coding.